

1  
2  
3  
4  
5  
6  
7  
8  
9  
10  
11  
12  
13  
14  
15  
16  
17  
18  
19  
20

**On site determination of trace metals in estuarine  
sediments by field-portable-XRF**

**Andrew Turner\*, Alex Taylor**

*School of Geography, Earth and Environmental Sciences, Plymouth University, Drake  
Circus, Plymouth PL4 8AA, UK*

\*Corresponding author

e-mail: [aturner@plymouth.ac.uk](mailto:aturner@plymouth.ac.uk)

[doi.org/10.1016/j.talanta.2018.08.024](https://doi.org/10.1016/j.talanta.2018.08.024)

Accepted 6 August 2018

Embargoed until 6 August 2019

21 **Abstract**

22 A portable x-ray fluorescence (XRF) spectrometer and mobile test stand have been  
23 employed to examine the feasibility of measuring trace metals in estuarine sediment in the  
24 field. The instrument was able to detect the trace metals: As, Cr, Cu, Pb, Sn and Zn; and the  
25 geochemical proxy metals: Ca, Fe, K and Rb; in both fresh and freeze-dried surficial samples  
26 from the Tamar and Tavy estuaries, southwest England, that had been emplaced in  
27 polyethylene bags over the detector window. The presence of interstitial water in fresh  
28 samples acted as both a diluent of sediment mass and an attenuator of incident and  
29 fluorescent x-rays, resulting in measured (fresh weight) metal concentrations that were  
30 significantly lower than corresponding (dry weight) concentrations derived from dry  
31 analyses. Gravimetric correction for fractional water content ( $f_w \sim 0.2$  to  $0.6$ ) gave rise to  
32 results that were within 20% of those derived from dry analyses with the exception of K,  
33 whose relatively low energy fluorescent x-rays were subject to significant attenuation from  
34 the aqueous medium; further x-ray attenuation was observed for both K and Ca through the  
35 sample bag, thereby limiting the usefulness of the approach for these metals. A relationship  
36 between the concentration of Rb and  $f_w$  in fresh samples suggests that Rb may be used as a  
37 proxy for interstitial water content through its covariance with sediment grain size.  
38 Accordingly, on site measurements of trace metals of sufficient fluorescent x-ray energies  
39 may be corrected empirically with respect to Rb in order to simultaneously account for  
40 variations in granulometry and mass contribution of water. On this basis, results from an  
41 axial transect of the Tamar and an intertidal transect in the Tavy were able to detect  
42 variations in trace metal concentrations that were consistent with known sources and  
43 geochemical behaviours.

44

45 **Keywords:** portable-XRF; estuarine sediments; trace metals; contaminants; on site

46

47 **1. Introduction**

48 Estuaries represent the river-ocean interface of the hydrosphere and play a key role in the  
49 transportation, modification and storage of materials and chemicals derived from natural  
50 erosion and anthropogenic inputs in the watershed (Regnier et al., 2014). Estuarine  
51 sediments are particularly significant vectors and reactors in this respect since they undergo  
52 considerable internal recycling through resuspension-deposition and provide a high surface  
53 area for the adsorption-desorption of a variety of chemicals (Turner and Millward, 2002).  
54 Trace metal(loid) contaminants, such as As, Cu, Pb and Zn, interact strongly with suspended  
55 and deposited estuarine sediment through a variety of processes, and concentrations in  
56 intertidal or subtidal deposits often provide an indication of the anthropogenic signature in  
57 the catchment (Kennish, 1998). Accordingly, measurements of trace metals in sediments  
58 form an integral component of many assessments of estuarine quality or status (Mucha et al.,  
59 2004; Azevedo et al., 2013; Cao et al., 2014).

60  
61 Conventionally, metals and metalloids (hereafter referred to as metals) in estuarine and  
62 coastal sediments are determined by a suitable spectrophotometric technique following total  
63 or quasi-total digestion of dried samples by flux fusion or combined acid attack (Wei and  
64 Haraguchi, 1999; Zhao et al., 2017). Analysis by inductively coupled plasma spectrometry or  
65 atomic absorption spectrometry, for example, is rapid and relatively straightforward, but  
66 digestion may be time- and resource-intensive and can generate considerable quantities of  
67 hazardous waste. Alternative, non-destructive approaches for measuring metals in sediments  
68 include neutron activation analysis and benchtop x-ray fluorescence (XRF) spectrometry  
69 (Al-Jundi, 2001; Alyazichi et al., 2017) but equipment may be expensive to run and,  
70 regarding the former, access to a nuclear reactor is required. Moreover, both sample  
71 preparation, involving milling and pelletisation or packing, and sample analyses are time-  
72 consuming.

73

74 With the miniaturisation of x-ray tubes, improvements in detector resolution and  
75 advancements in signal processing capability, portable, energy-dispersive XRF has gained  
76 increasing use for the rapid, cost-effective and non-destructive analysis of metals in  
77 particulate geosolids over the past two decades (Radu and Diamond, 2009; Quiroz-Jiménez  
78 and Roy, 2017). Minimal sample processing (sieving and drying) has allowed a high  
79 throughput of samples in the laboratory, but measurements may also be performed in the  
80 field if material is sufficiently fine, homogeneous and dry (Higueros et al., 2012). In this  
81 respect, estuarine sediments are more challenging because of a relatively high content of  
82 interstitial water. Thus, besides the risk of damaging sensitive components within the  
83 detector window, water acts as a diluent of sediment mass and an attenuator of incident  
84 (primary) and fluorescent (secondary) x-ray, effects that reduce signal intensity and tend to  
85 underestimate true (absolute) concentrations.

86

87 Attempts have been made to measure metals in sediment samples in the fresh or part-dried  
88 state by portable XRF, in both the laboratory and in the field, with results deemed to be of  
89 sufficient quality to screen for heavy metal contamination or to aid decision-making for  
90 management purposes (Stallard et al., 1995; Kirtray et al., 1998; Ge et al., 2001; Lemiere et  
91 al., 2014; Mejía-Piña et al., 2017). However, the significance of water and suitable means for  
92 its correction are rarely addressed in a systematic or quantitative manner that allow absolute,  
93 dry weight concentrations to be accurately predicted. To this end, we evaluate the potential  
94 of a battery-powered Niton XRF instrument coupled with a mobile test stand for the field  
95 measurement of trace metals in estuarine sediments. Specifically, the effects of x-ray  
96 attenuation by suitable containers and by interstitial water are examined in controlled  
97 experiments in the laboratory, with results compared with those obtained from an optimised  
98 geometry whereby samples had been freeze-dried and milled prior to packing into

99 customised XRF sample cups. A configuration of the instrument and stand is tested in the  
100 field, with means of correcting on site results for water content explored which are based on  
101 gravimetric measures or the use of analyte proxies for moisture.

102

## 103 **2. Materials and methods**

### 104 *2.1. XRF instrumentation and configuration*

105 In the current study, samples were analysed for various metals either in the laboratory or in  
106 the field using a Niton XL3t 950 He GOLDD+ portable XRF spectrometer. Measurements  
107 were conducted in a ‘mining’ mode and with a beam width of 8 mm (equivalent to a  
108 measurement area of 50 mm<sup>2</sup>) for a total time of 60 s, comprising successive counting  
109 periods of 30 s at 50 kV/40 μA (main filter), 15 s at 20 kV/100 μA (low filter) and 15 s at 50  
110 kV/40 μA (high filter). This mode is capable of detecting more than 20 elements in  
111 particulate geosolids (from K to Bi) but here we focus on trace metals that were readily  
112 detected in a preliminary study of estuarine sediments (As, Cr, Cu, Pb, Sb, Sn, Zn; Turner et  
113 al., 2017) as well as metals that act as potential geochemical proxies or indicators of  
114 analytical performance (Ca, Fe, K, Rb).

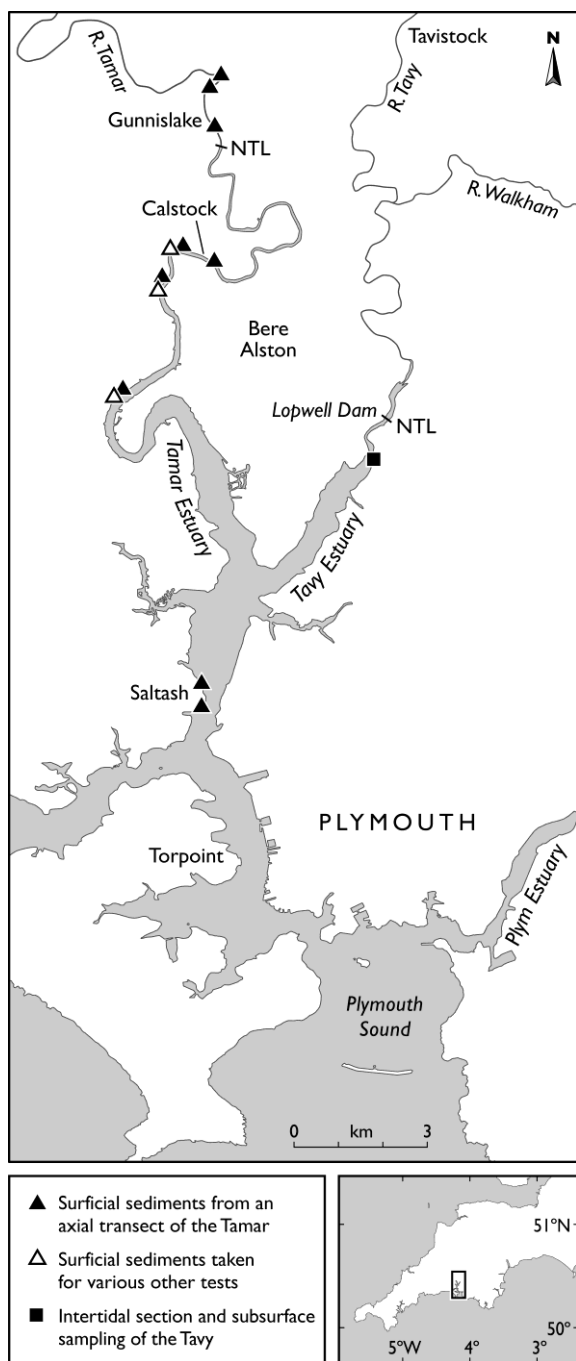
115

116 In the laboratory, the instrument was configured nose-upwards in a 4000 cm<sup>3</sup> accessory  
117 stand and activated remotely through a laptop and at an operator distance of 2 m. In the field,  
118 the instrument was configured nose-upwards in a 300 cm<sup>3</sup> portable test stand (described in  
119 detail elsewhere; Turner, 2017) and activated and operated likewise. Spectra arising from  
120 sample counting were quantified by fundamental parameter coefficients to yield metal  
121 concentrations in μg g<sup>-1</sup> and with a measurement counting error of 2σ (95% confidence) that  
122 were downloaded to the laptop via Niton data transfer (NDT) software.

123

### 124 *2.2. Sampling and sample characteristics*

125 Estuarine sediment samples were collected from the Tamar and its tidal tributary, the Tavy.  
126 The watershed of the Tavy and the upper catchment of the Tamar are dominated by  
127 moorland, managed forest and agricultural land but remain highly contaminated by various  
128 trace metals (and mainly As and Cu) from historical mining activities, while the lower  
129 catchment of the Tamar is partly urbanised and supports various facilities for the  
130 maintenance and repair of boats and ships. Fine, surficial (depth < 5 mm) intertidal muds and  
131 silts were targeted at the locations shown in Figure 1 and during 2017 and early 2018 in  
132 order obtain a variety of relatively homogeneous materials that required minimal processing.  
133 Specifically, (i) a number of samples were collected from the Tamar and Tavy as and when  
134 required in order to undertake various tests in the laboratory, (ii) a field transect was  
135 undertaken along the axis of the Tamar at nine sites from above its tidal limit to about 5 km  
136 from the mouth (including locations known to be impacted by metal inputs from adits and  
137 streams), and (iii) a ~ 20 m cross section of the intertidal zone was conducted on site in the  
138 Tavy estuary at a location bordered by saltmarsh; here, sampling was undertaken at 3 m  
139 intervals (measured using a 30 m tape measure) and included a number of anoxic, subsurface  
140 sediments that were accessed from pits dug into the substrate.



141

142 **Figure 1: Sampling locations in the Tamar and Tavy estuaries, southwest England.**

143 **NTL = normal tidal limit.**

144

145 About 50 to 100 g of material were collected with a plastic trowel and transferred directly

146 into a clear, minigrip, re-sealable polyethylene bag (1.25 g, 12 cm x 9 cm below the seal;

147 Polybags Ltd, Greenford UK) for direct measurement in the field or for return to the

148 laboratory and subsequent testing. Bags were selected on the basis of rigidity and strength,

149 thickness 50  $\mu\text{m}$  per face), water-tightness, sample accessibility and material purity.  
150 Regarding the latter, analysis by the Niton XL3t in a low density ‘plastics’ mode and with  
151 thickness correction revealed no metallic contamination of clear polyethylene but the  
152 presence of small quantities of Ti and Ba in the white labelling panel. Once bagged, samples  
153 were squeezed gently in order to detect any larger extraneous particles, like shell fragments,  
154 grit and plant debris. Occasional particles were eliminated with tweezers, with sieving  
155 through a 1 mm plastic mesh and into a polyethylene bowl required in cases where larger  
156 solids were more abundant.

157

158 Particle size analysis was performed on aliquots of selected samples using a Malvern  
159 Instruments Mastersizer 2000 equipped with a He-Ne laser. Briefly, subsamples were  
160 introduced to a Hydro-G sample unit holding a 1 L solution of 0.1% sodium  
161 hexametaphosphate in Elga ultrapure water (UPW). The contents were continuously stirred  
162 to ensure proper resuspension and subsequently ultrasonically dispersed before successive  
163 30-s measurements ( $n = 5$ ) were performed in the diffraction cell. Results revealed volume  
164 weighted means in the range 50 to 150  $\mu\text{m}$ , and 5<sup>th</sup> and 95<sup>th</sup> percentile values of about 5  $\mu\text{m}$   
165 and between about 200 to 700  $\mu\text{m}$ , respectively.

166

### 167 *2.3. Sediment testing by XRF in the laboratory*

168 The effects of interstitial water on XRF measurements through both contribution to sample  
169 mass and x-ray attenuation were examined on two samples of different metallic composition  
170 from the Tamar estuary. After weighing on a Sartorius two-figure balance, bagged samples  
171 were placed sideways and with the labelling panel facing upwards over the detector window,  
172 ensuring that the depth of material was at least 8 mm (an assumed critical thickness of a  
173 sediment-water mixture; Parsons et al., 2013). With the accessory stand shield closed,  
174 samples were counted six times at the same (50 mm<sup>2</sup>) location in order to determine



175 measurement precision and a further six times at different locations in order to evaluate  
176 spatial heterogeneity.  
177

178 Samples were subsequently freeze-dried in an Edwards Super Modulyo for 96 h before being  
179 reweighed, homogenised (by gently shaking and manually kneading the bagged contents),  
180 and reanalysed six times at one location and six times at multiple locations. Increasing  
181 quantities of UPW were then added in order to wet samples with the contents in their  
182 original bags reweighed and reanalysed by XRF as above after each aqueous addition. Here,  
183 water was dispensed using a Jencons Sealpette 1 ml micropipette and dispersion of water  
184 throughout the sample was accomplished by careful manual manipulation of the bagged  
185 contents and subsequent lateral shaking at 500 rpm for up to 30 minutes on an Ika KS 130  
186 shaker. Based on preliminary investigations into the moisture content of intertidal mud and  
187 practical constraints that included the ability to wet sediments homogeneously, the fraction of  
188 added UPW to total mass was varied between about 0.2 and 0.7.  
189

190 Any effects on XRF measurements arising from particle size and mineralogical variations  
191 within and between samples were evaluated by analysing a number of dried sediments from  
192 the Tamar and Tavy estuaries ( $n = 12$ ) in re-sealable bags both before and after milling (to <  
193 50  $\mu\text{m}$ ). The latter was accomplished in a series of 80 mL agate bowls, each containing five  
194 20 mm agate milling balls, using a Fritsch planetary mill (model Pulverisette 5) at 300 rpm  
195 for 3 min. Primary and secondary x-ray attenuation by the re-sealable bags was tested on a  
196 number of reference materials (NIST 2709, Agricultural Soil; MSH101, loam; GBW07318,  
197 stream sediment) and milled, freeze-dried Tamar sediments that had been packed into  
198 individual, polyethylene XRF sample cups (Chemplex series 1400, 21-mm internal  
199 diameter) and collar-sealed with 3.6  $\mu\text{m}$  SpectraCertified Mylar polyester film. Here,

200 samples were analysed six times directly through the polyester film and then six times  
201 through an additional 50  $\mu\text{m}$  layer of polyethylene cut from the face of a bag.

202

203 Dried and milled materials prepared in customised sample cups eliminate the absorptive and  
204 matrix effects of moisture and polyethylene and minimise variations in particle size or  
205 texture. XRF results obtained through direct the analysis of samples processed this way  
206 therefore afford optimal measures of absolute, dry weight concentrations, while reference  
207 materials processed and analysed similarly serve as a measure of the accuracy of the  
208 technique. To this end, mean measured metal concentrations and certified concentrations for  
209 three reference geosolids, compared in Table 1 on a dry weight basis ( $[\text{Me-dw}]$ ,  $\mu\text{g g}^{-1}$  dw),  
210 reveal agreement that is always better than 25% apart from Cr and K in NIST 2079  
211 (agreement within 30%), and repeatability that is better than 10% in most cases.

212

213 **Table 1: Certified and measured concentrations of metals ( $[\text{Me-dw}]$ ,  $\mu\text{g g}^{-1}$  dw) in three**  
214 **reference materials. Errors represent 95% confidence intervals arising from six**  
215 **measurements (measured) or an unspecified number of measurements (certified) and <**  
216 **LOD denotes a mean concentration below the limit of detection.**

reference material	metal	certified, $\mu\text{g g}^{-1}$ dw	measured, $\mu\text{g g}^{-1}$ dw
NIST 2709	As	10.5 $\pm$ 0.3	9.6 $\pm$ 1.2
	Ca	19,100 $\pm$ 900	17,800 $\pm$ 318
	Cr	130 $\pm$ 9	92.6 $\pm$ 10.8
	Cu	33.9 $\pm$ 0.5	28.1 $\pm$ 5.2
	Fe	33,600 $\pm$ 700	34,000 $\pm$ 157
	K	21,100 $\pm$ 600	15,600 $\pm$ 179
	Pb	17.3 $\pm$ 0.1	15.2 $\pm$ 2.2
	Rb	99.0 $\pm$ 3	91.3 $\pm$ 2.1
	Zn	103 $\pm$ 4	101 $\pm$ 5.4
MSH101	As	1090 $\pm$ 16.7	1220 $\pm$ 11.3
	Zn	1100 $\pm$ 16.8	1260 $\pm$ 15.8
GBW07318	As	18 $\pm$ 2	22.2 $\pm$ 5.5
	Cr	243 $\pm$ 16	198 $\pm$ 8.5
	Cu	66 $\pm$ 6	60.3 $\pm$ 7.8
	Pb	66 $\pm$ 7	58.5 $\pm$ 5.7
	Rb	87 $\pm$ 7	83.4 $\pm$ 0.9
	Sn	9.5 $\pm$ 1.7	<LOD
	Zn	165 $\pm$ 15	174 $\pm$ 4.0
	Ca	25,000 $\pm$ 710	20,600 $\pm$ 325
	K	19,200 $\pm$ 830	16,800 $\pm$ 194

217

218

219

### 220 3. Results and Discussion

#### 221 3.1. Measures of LOD, precision and heterogeneity for sediment in the fresh and dried states

222 Measurement limits of detection (LOD) and measures of precision and heterogeneity for the  
223 different metals arising from multiple analyses ( $n = 6$ ) of three bagged Tamar estuary  
224 samples are presented in Table 2. LODs are given both on a fresh weight basis ([Me-fw],  $\mu\text{g}$   
225  $\text{g}^{-1}$  fw), as would be tested in the field, and on a dry weight basis ([Me-dw],  $\mu\text{g g}^{-1}$  dw) after  
226 freeze-drying in the laboratory. LOD is based on the counting error and defined as  $3\sigma$ , and is  
227 either reported directly by the instrument where an element is undetected or is derived from  
228 multiplication of  $2\sigma$  by 1.5 when detection is achieved. For a given counting time and  
229 sample thickness (above a critical depth), LODs are specific to the precise composition of  
230 the sample (and, in particular, the relative abundance of metals whose fluorescent x-ray

231 energies are similar) and limits reported in the Table, based on the lowest mean values  
232 among the three samples tested, should be regarded as approximate. Thus, in the dry state,  
233 LODs range from  $< 20 \mu\text{g g}^{-1}$  for As, Cd, Pb and Rb to  $> 100 \mu\text{g g}^{-1}$  for Ca, Co, Fe and K,  
234 while in the fresh state LODs are always lower than corresponding values after freeze-drying  
235 and range from  $< 10 \mu\text{g g}^{-1}$  for As, Cd, Pb and Rb to  $> 100 \mu\text{g g}^{-1}$  for Ca, Fe and K. Lower  
236 LODs in the fresh state may be related to the ability to place a wet paste or slurry closer to  
237 and flatter against the detector window than a dried, particulate material (Turner et al.,  
238 2017), but once concentrations in fresh samples had been normalised to a dry weight basis  
239 ( $[\text{Me-dw}^*]$ ,  $\mu\text{g g}^{-1} \text{dw}^*$ ) by correcting for the fraction of water present,  $f_w$ :

240

$$241 \quad [\text{Me-dw}^*] = [\text{Me-fw}]/(1-f_w) \quad (1)$$

242

243 LODs were, in general, considerably greater than corresponding limits when analysed dry.  
244 Within these constraints, As, Ca, Cu, Fe, K, Pb, Rb, Sn and Zn were detected in all cases and  
245 in both the fresh and dry states and Cr was detected in most cases when fresh and in all cases  
246 when dry.

247

248 **Table 2: Limits of detection (LOD) and measures of precision and spatial heterogeneity**  
249 **for metals in three Tamar estuary sediments analysed six times in resealable bags in**  
250 **the fresh state and after freeze-drying. LOD refers to the lowest mean value while**  
251 **precision and heterogeneity are reported as a range of values (with the exception of Cr**  
252 **in the fresh state;  $n = 1$  or  $2$ ).**

metal	fresh			dry		
	LOD, $\mu\text{g g}^{-1}$ fw	precision, %	heterogeneity, %	LOD, $\mu\text{g g}^{-1}$ dw	precision, %	heterogeneity, %
As	6.8	1.5-9.6	8.2-19.0	15.6	1.0-4.8	5.4-12.6
Ca	189	2.9-4.7	7.5-22.3	618	2.6-2.7	6.1-10.2
Cr	33.9	9.6	9.6; 13.0	47.2	14.9-18.4	18.3-38.1
Cu	14.9	2.2-16.7	8.9-13.0	29.6	1.3-3.6	4.2-7.7
Fe	197	0.6-1.0	2.0-8.0	515	0.3-0.6	3.0-8.5
K	210	2.4-3.7	5.6-15.1	697	1.3-1.5	3.2-5.5
Pb	6.5	2.0-5.0	3.2-13.4	14.7	1.7-2.1	2.7-5.9
Rb	3.0	1.4-2.5	4.0-11.2	7.7	0.7-2.1	1.5-2.9
Sn	14.1	6.5-25.4	16.2-26.3	27.8	4.0-12.4	11.0-18.7
Zn	12.1	2.8-4.4	1.7-12.3	27.0	2.0-2.6	2.9-8.1

254

255 Precision is shown in Table 1 as the relative standard deviation (rsd, %) resulting from  
256 repeated measurements of the same 50 mm<sup>2</sup> area of a bagged sample and for a given metal is  
257 presented as the minimum and maximum value arising from the three samples tested. When  
258 analysed fresh, precision ranges from < 1% for Fe in all three samples to > 15% for Cu and  
259 Sn in one case each. In the dry state, the minimum and maximum precisions are always  
260 better (or rsds always lower) than corresponding values in the fresh state, despite greater  
261 analytical sensitivity achieved for the latter.

262

263 Heterogeneity, defined as the rsd of multiple measurements performed at different 50 mm<sup>2</sup>  
264 locations of the same sample, is also presented in Table 1 in terms of minimum and  
265 maximum values. In nearly all cases, spatial heterogeneity is greater than corresponding  
266 precision, with differences in some cases about an order of magnitude. Heterogeneity may be  
267 attributed to the variation of a number of parameters across a given sample contained within  
268 a re-sealable bag that include material thickness, water content and dispersion, grain size and  
269 porosity and sediment settlement (see below), as well as any inherent variations in the  
270 distributions of trace or geochemical metals themselves. Without further material processing,  
271 heterogeneity is considered a better indicator of variation than precision and is, therefore,  
272 adopted as a default measure in all further testing.

273

274 3.2. *Effects of sample milling on metal concentrations returned by XRF*

275 In order to explore the sources of analyte spatial variation further, a greater variety of  
276 samples collected from the region on a number of occasions ( $n = 12$ ) was analysed as above  
277 and at different locations with respect to the face of the re-sealable bag after freeze-drying  
278 and then after milling to a finer and more homogenous powder. Although we observed  
279 greater variability within the same sample before milling, mean concentrations showed good  
280 agreement with corresponding mean concentrations after homogenisation. Thus, regression  
281 coefficients defining the association of the two measures exceeded 0.9 for all metals  
282 considered with the exception of Cr and Fe (where the range in concentrations tested was  
283 relatively small), with slopes that were within 10% of unit value in all cases with the  
284 exception of Pb (Table 3). These observations suggest that spatial variation in metal  
285 concentrations is at least partly associated with an inherent variation within samples when  
286 dried (including variations in grain size and mineralogy) but that averaging of multiple  
287 analyses without milling generally gives a good measure of overall concentration. In the  
288 fresh state, we surmise that greater variation arises from the presence and heterogeneous  
289 dispersion of water within the sample, whose effects on XRF measurements are examined in  
290 more detail below.

291

292 **Table 3: Slopes and regression coefficients defining the relationships between mean**  
293 **metal concentrations ([Me-dw],  $\mu\text{g g}^{-1}$  dw;  $n = 6$ ) measured on 12 dried samples before**  
294 **and after milling.**

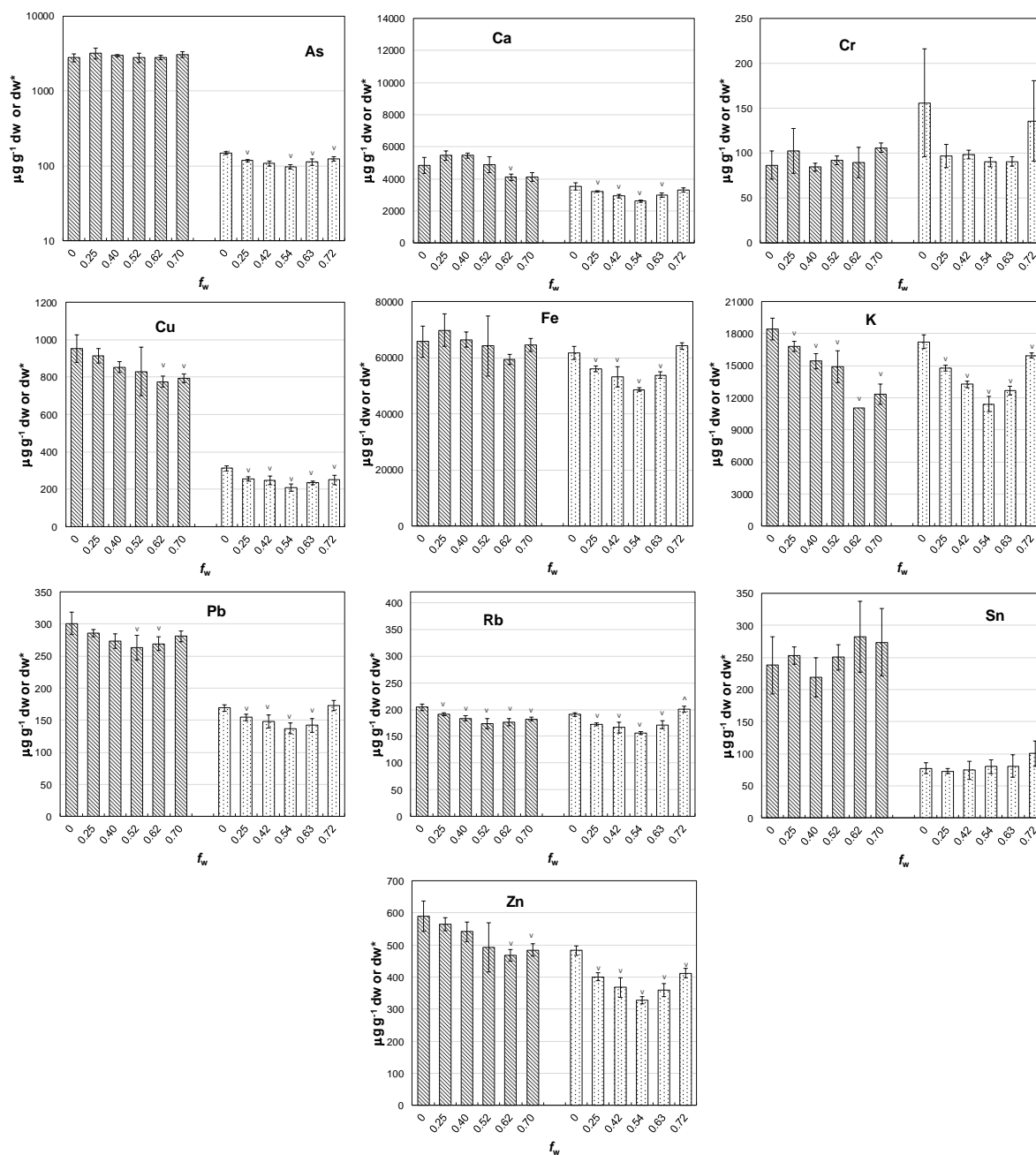
metal	Slope	$r^2$
As	1.017	0.980
Ca	0.904	0.992
Cr	0.909	0.238
Cu	0.994	0.944
Fe	1.009	0.747
K	1.003	0.998
Pb	0.859	0.999
Rb	1.038	0.950
Sn	0.966	0.968
Zn	0.978	0.980

295

296

### 297 3.3. Effects of water on metal concentrations returned by XRF

298 With the effects of moisture on LOD and measurement variation established, the effects of  
 299 interstitial water on metal concentrations returned by the XRF were investigated more  
 300 systematically. Figure 2 shows the results of XRF analyses performed on two Tamar estuary  
 301 samples, originally in the dry state, over a range of  $f_w$  values that were engendered by  
 302 incremental additions of UPW. Metal concentrations are shown on a dry weight basis as  
 303 determined directly after freeze-drying ( $[Me-dw]$ ,  $\mu\text{g g}^{-1} dw$ ) or on a dry weight basis but as  
 304 determined in the wetted state and after correction for the mass of water present ( $[Me-dw^*]$ ,  
 305  $\mu\text{g g}^{-1} dw^*$ ; equation 1). Where errors were relatively high or variable (e.g. Sn in both  
 306 samples and As, Cr and Fe in one sample), there were no clear differences in mean metal  
 307 concentrations over the range of water content tested. However, in the majority of cases  
 308 there was a reduction in mean concentration with increasing water content over all or part of  
 309 the range tested that was often significant according to one-way ANOVA and a post-hoc  
 310 Tukey test ( $\alpha = 0.05$ ). Specifically, there was generally a minimum in dry weight elemental  
 311 concentration at an  $f_w$  of about 0.5 or 0.6 and a subsequent increase in concentration with  
 312 further additions of UPW. This type of distribution can be understood from the interplay of  
 313 two competing effects: namely, the attenuation of x-rays by the interstitial medium and the  
 314 settlement of sediment in a slurry-type preparation.



316  
 317 **Figure 2: Dry weight metal concentrations in two Tamar estuary sediment samples**  
 318 **(shaded differently) that were analysed in the dry state ([Me-dw],  $\mu\text{g g}^{-1} \text{dw}$ ;  $f_w = 0$**   
 319 **only) and subsequently in the fresh state after incremental additions of UPW ([Me-**  
 320 **dw\*],  $\mu\text{g g}^{-1} \text{dw}^*$ ; equation 1). Errors represent one standard deviation about the mean**  
 321 **of six measurements undertaken at different sample locations and v or ^ indicate mean**  
 322 **concentrations that are significantly lower or higher than corresponding mean**  
 323 **concentrations reported for the dry state (one-way ANOVA,  $\alpha = 0.05$ ).**



324  
325 Because x-rays are attenuated (through photoelectric absorption and scattering) to a  
326 considerably greater extent by liquid water than by air, the presence of interstitial water  
327 reduces the energy available for sample excitation and decreases the sensitivity of the  
328 analysis, at least when converted to a dry weight basis (Ge et al., 2005). Attenuation of this  
329 nature will affect metals differently in terms of analytical sensitivity and measurement error  
330 depending on the primary x-ray energies required for excitation (i.e. low, main or high  
331 filters; see above) but its overall impact should be directly related to the percentage of water  
332 present. The water-attenuation of fluorescent x-rays that are registered by the detector results  
333 in lower counts and apparent concentrations, an effect whose magnitude is predicted to be  
334 metal-specific (and dependent on the energies of the principal lines used in detection) and  
335 directly related to the quantity of water present.

336  
337 The results in Figure 2 are partly consistent with secondary x-ray attenuation in that  
338 reductions in [Me-dw\*] with increasing  $f_w$  are most pronounced for K, whose  $K_{a1}$  line energy  
339 is the lowest among the elements considered (3.31 keV), and not evident for Sn, whose  $K_{a1}$   
340 energy line is the highest (25.27 keV). However, the effects of x-ray attenuation also appear  
341 to be offset to differing extents above a fractional water content of about 0.5 to 0.6. Here, we  
342 attribute an increase in apparent concentration to the settlement of material from slurries of a  
343 relatively high water content during the analysis. Partial separation of solid and aqueous  
344 media results in analytes that are closer to the detector window and a reduced thickness of  
345 water for primary and secondary x-ray attenuation compared with samples where sediment is  
346 in a more homogenous suspension. Overall, therefore, analysis of fine sediment samples in  
347 the fresh state appears to be limited to  $f_w$  values of about 0.5 to 0.6 before the effects of  
348 settlement become evident, with dry weight-normalised results that are within 20% of results  
349 when analysed dry with the exception of K.

350  
351  
352  
353  
354  
355  
356  
357  
358  
359  
360  
361  
362  
363  
364  
365  
366  
367  
368  
369  
370  
371  
372  
373  
374

#### 3.4. Attenuation of fluorescent x-rays by polyethylene

Because sediment samples are contained in polyethylene bags, it was necessary to evaluate the potential impacts on metal measurements arising from x-ray attenuation by polyethylene. Here, various milled samples ( $n = 6$ ; including three reference sediments and soils) contained in XRF cups were analysed at different locations through the  $\sim 4 \mu\text{m}$  polyester retaining film both with and without a  $50 \mu\text{m}$  layer of polyethylene derived from a resealable bag placed above the detector window. Polyethylene has a similar mass attenuation coefficient to water across the energy range of 0 to 50 keV (Hubbell and Seltzer, 1996) but its thickness in the current context is considerably more uniform both within and between samples. Table 4 compares results for each element considered in terms of the slope and linear regression coefficient arising from mean concentrations ( $[\text{Me-dw}]$ ,  $\mu\text{g g}^{-1} \text{dw}$ ) in the presence and the absence of polyethylene. In all cases, regressions were highly significant ( $p < 0.01$ ) and coefficients exceeded 0.93, with slopes in only three cases deviating from unit value by more than 5%; specifically, those for Ca, Cr and K were about 0.80, 0.86 and 0.74, respectively (equivalent to attenuations of about 20%, 14% and 26%, respectively), reflecting the relatively low energies of their respective K lines ( $K_{\alpha 1} = 3.69 \text{ keV}$ ,  $5.41 \text{ keV}$  and  $3.31 \text{ keV}$ ).

**Table 4: Slopes and regression coefficients defining the relationships between mean metal concentrations ( $[\text{Me-dw}]$ ,  $\mu\text{g g}^{-1} \text{dw}$ ;  $n = 6$ ) measured on six dried soil and sediment samples (including three reference materials) in the presence and absence of a  $50 \mu\text{m}$  layer of polyethylene.**

metal	slope	$r^2$
As	0.969	1.000
Ca	0.798	0.998
Cr	0.863	0.937
Cu	0.972	0.998
Fe	0.957	0.993
K	0.735	0.984
Pb	0.958	1.000
Rb	0.954	0.996
Sn	0.956	1.000
Zn	0.988	1.000

375

376 *3.5. Combined effects of water and polyethylene*

377 The results of the present tests performed on fine estuarine sediments are qualitatively  
378 consistent with results obtained for floodplain soils by Parsons et al. (2013). That is, a  
379 reduction in apparent concentration is observed with increasing interstitial water content and  
380 in the presence of a polyethylene barrier, effects that are most pronounced for lighter  
381 elements with relatively low energy x-ray emission lines like Ca and K. Quantitatively,  
382 however, the impacts of attenuation by water and polyethylene on sediment appear to be  
383 lower than those observed for soils and agreement between measurements performed on  
384 fresh and dried sediments is within 20% up to a fractional water content of about 0.6 for  
385 elements whose atomic mass is greater than Ca.

386

387 As means of a summary thus far, Table 5 compares portable XRF results obtained from  
388 multiple analyses of a Tamar estuary sample that had undergone each step of processing  
389 described above. Specifically, concentrations of metals are shown when sediment was  
390 analysed (i) bagged and in the fresh state, and after normalisation for interstitial water  
391 content according to equation 1, (ii) bagged and after freeze-drying, (iii) bagged and after  
392 milling, and (iv) packed into a sample cup after milling. In general, results become  
393 progressively more precise through each stage and as the optimal measure of absolute  
394 concentration is approached. Significantly, however, results obtained when the sample was  
395 analysed fresh and bagged and corrected for moisture are statistically indistinguishable from

406 optimal results (according to a series of paired *t*-tests;  $\alpha = 0.05$ ) for all metals with the  
 407 exception of Cu, Ca and K; here, concentrations were about 15%, 35% and 45% lower when  
 408 analysed fresh, with the relatively large discrepancies for the latter metals reflecting the  
 409 combined effects of secondary x-ray attenuation by both water and polyethylene described  
 400 above.

401

402 **Table 5: A comparison of metal concentrations in a sample of Tamar sediment that had**  
 403 **been analysed fresh and normalised for moisture content (equation 1), analysed dry,**  
 404 **analysed after milling and analysed after milling and packing in an XRF sample cup.**  
 405 **Errors represent one standard deviation about the mean of 6 or 7 analyses performed**  
 406 **at different locations with respect to the sample bag or polyester surface.**

	fresh	dry	dry-milled	dry-milled-packed
metal	$\mu\text{g g}^{-1} \text{dw}^*$	$\mu\text{g g}^{-1} \text{dw}$	$\mu\text{g g}^{-1} \text{dw}$	$\mu\text{g g}^{-1} \text{dw}$
As	116 $\pm$ 6.7	128 $\pm$ 4.8	128 $\pm$ 3.1	130 $\pm$ 5.7
Ca	3800 $\pm$ 321	4200 $\pm$ 112	4430 $\pm$ 122	5600 $\pm$ 60.6
Cr	107 $\pm$ 10	102 $\pm$ 21.8	90.8 $\pm$ 10.5	114 $\pm$ 17.6
Cu	234 $\pm$ 23	284 $\pm$ 14.9	264 $\pm$ 12.2	273 $\pm$ 11.6
Fe	52,900 $\pm$ 2220	53,300 $\pm$ 889	50,900 $\pm$ 597	54,300 $\pm$ 326
K	11,300 $\pm$ 659	16,200 $\pm$ 713	15,000 $\pm$ 289	20,700 $\pm$ 314
Pb	147 $\pm$ 4.7	151 $\pm$ 4.7	149 $\pm$ 2.6	154 $\pm$ 2.4
Rb	166 $\pm$ 4.2	170 $\pm$ 4.8	165 $\pm$ 2.7	169 $\pm$ 2.0
Sn	84.3 $\pm$ 22.8	82.2 $\pm$ 11.7	86.4 $\pm$ 10.0	89.0 $\pm$ 6.0
Zn	386 $\pm$ 34.5	427 $\pm$ 11.7	407 $\pm$ 10.2	429 $\pm$ 12.6

408

### 409 3.6. XRF analysis on site

410 Within the constraints and variations associated with the analysis of fresh sediments, the  
 411 XRF spectrometer was tested on site during two field surveys. Thus, firstly, an axial transect  
 412 of the Tamar estuary was undertaken from above its tidal limit to about 5 km from its mouth  
 413 and at the nine locations shown in Figure 1. Here, the instrument, portable test stand and  
 414 laptop were driven to the foreshore where they were configured directly, or with the use of  
 415 the equipment carry cases, on a flat, firm surface. Surficial samples were collected with a

416 plastic trowel, manually checked for extraneous material, and analysed directly and at six 50  
417 mm<sup>2</sup> locations in resealable polyethylene bags under the operating conditions defined above.  
418 Provided that samples were readily accessible, the time required at each site was less than 20  
419 minutes for two trained operators working simultaneously.

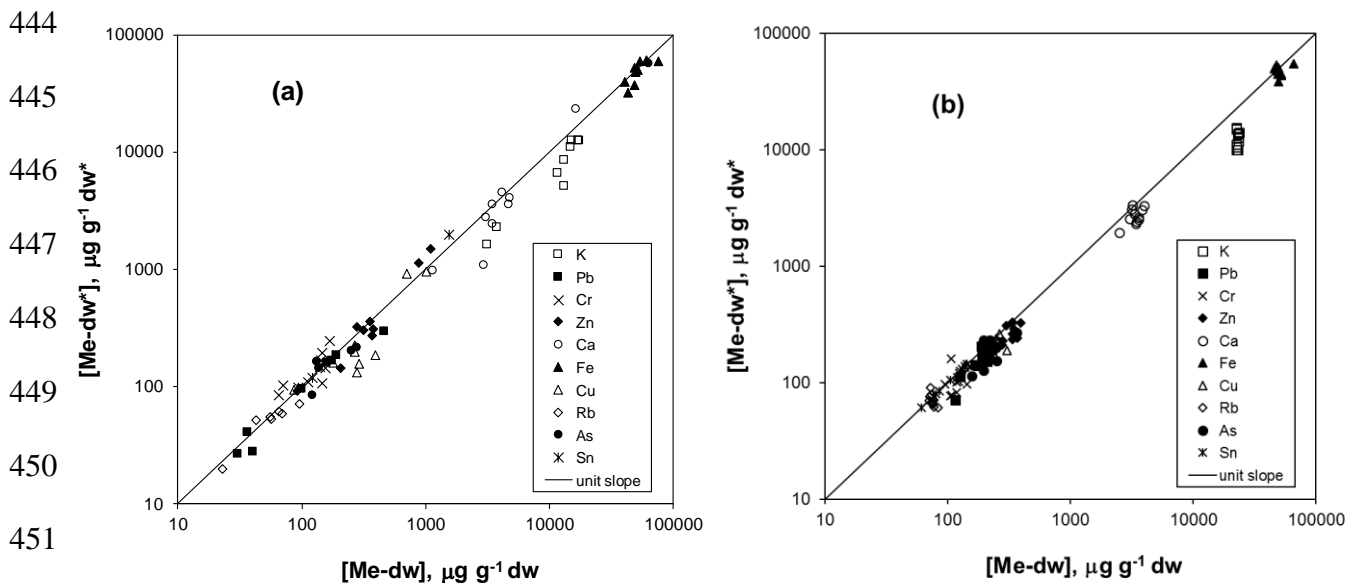
420

421 Secondly, a transect of the intertidal zone on the Tavy estuary at the location shown in  
422 Figure 1 was undertaken from the saltmarsh to near the low water mark; this survey also  
423 included sampling below the sediment surface from pits dug using a garden spade. As above,  
424 the equipment was set up on the foreshore and each sample was analysed directly and at six  
425 locations. Here, once the equipment had been set up on site, a throughput of about six to  
426 eight samples per hour was readily accomplished by two operators, with a range of  
427 measurements, in theory, limited by the life of the laptop and XRF batteries (about two and  
428 four hours, respectively). On return to the laboratory, samples from both surveys were  
429 weighed, freeze-dried, re-weighed and re-analysed in the laboratory accessory stand.

430

431 The results of the axial and inter-tidal surveys are summarised in Figure 4 in terms of  
432 concentrations determined on site and after correction for water content, ([Me-dw\*],  $\mu\text{g g}^{-1}$   
433 dw\*; equation 1), versus concentrations determined in the laboratory and after freeze-drying,  
434 ([Me-dw],  $\mu\text{g g}^{-1}$  dw). Here, linear regression analysis has been performed on all metals  
435 combined since the range of concentrations encountered for many individual elements was  
436 too small to determine any degree of association. Thus, overall, the slopes of the best-fit  
437 lines were within 15% of unit value and regression coefficients exceeded 0.95 for both  
438 surveys, with better fits that were closer to unit value resulting when data for Ca and K were  
439 excluded from the analysis. The mean and one standard deviation of  $f_w$  for the axial and  
440 intertidal transects were  $0.555 \pm 0.09$ . and  $0.559 \pm 0.123$ , respectively, suggesting that a  
441 value of close to 0.5 affords a good approximation of this parameter, at least in the current

442 environments, when gravimetric analysis is not possible or an immediate assessment of  
 443 sediment geochemistry or contamination is required.



453 **Figure 4: Mean concentrations of metals measured on site and subsequently corrected**  
 454 **for fractional water content according to equation 1 ( $[Me-dw^*]$ ,  $\mu g g^{-1} dw^*$ ;  $n = 6$ )**  
 455 **versus corresponding mean concentrations measured after freeze-drying ( $[Me-dw]$ ,  $\mu g$**   
 456  **$g^{-1} dw$ ;  $n = 6$ ) in the (a) Tamar estuary and (b) Tavy estuary. Errors are not shown for**  
 457 **clarity and the solid line represents unit slope. Results of linear regression analysis**  
 458 **were as follows: (a)  $y = 0.916x$ ,  $r^2 = 0.974$ ,  $p < 0.001$ ; (b)  $y = 0.870x$ ,  $r^2 = 0.954$ ,  $p < 0.001$ ;**  
 459 **and after exclusion of Ca and K data were: (a)  $y = 0.923x$ ,  $r^2 = 0.982$ ,  $p < 0.001$ ; (b)  $y =$**   
 460  **$0.930x$ ,  $r^2 = 0.985$ ,  $p < 0.001$ .**

461  
 462 *3.7. Rb as a proxy for grain size and water content*

463 Employing XRF to determine metal concentrations in marine sediment cores, Tjallingii et al.  
 464 (2007) suggest using Cl as a proxy for sea water content when sections are analysed in the  
 465 wet state. However, the XL3t series of Niton analysers are not calibrated for Cl in modes  
 466 designed for particulate geosolids. Moreover, should the Cl intensity be quantified, estuaries  
 467 are characterised by such strong spatial and temporal variations in salinity that measurement

468 of the latter in the interstitial environment would also be required. Accordingly, an indirect  
469 means of estimating the interstitial water content on site was explored based on the premise  
470 that it bears some relationship with sediment porosity, hence grain size.

471

472 Aluminium is often employed as a sediment grain size normaliser (Nolting et al., 1999; Din,  
473 1992) but is too light to be analysed by conventional portable XRF unless measurements are  
474 performed in a helium atmosphere. Iron has also been employed to compensate for grain size  
475 variations (Loring, 1991) but in the current setting this metal has a strong anthropogenic  
476 signal from historical mining activities (Mighanetara et al., 2009). An alternative normaliser  
477 that has been used in some studies is Rb, whose concentration in sediment bears an inverse  
478 relationship with grain size through substitution for K in fine-grained clays and whose  
479 distribution is unaffected by anthropogenic inputs (Rae, 1995; Turner and Lewis, 2018).

480 With respect to portable XRF, Rb has the additional advantages of being easy to detect and  
481 relatively little affected by water or polyethylene attenuation.

482

483 In Figure 5, the concentration of Rb determined in sediment in the fresh state ( $[Rb-f_w]$ ,  $\mu\text{g g}^{-1}$   
484  $f_w$ ) during the axial transect of the Tamar and the inter-tidal transect of the Tavy is plotted  
485 against  $1 - f_w$  determined subsequently by gravimetry. For the inter-tidal transect, where  
486 material is likely similar in geology and origin across the relatively small area surveyed, the  
487 goodness of fit is excellent; for the axial transect, encompassing a wider range of lithological  
488 materials and sources, the data are more scattered but the fit is still significant. This  
489 relationship is not predicted from simple porosity considerations alone where an increase in  
490 grain size of a given shape is accompanied by decreasing void space for the occupation by  
491 interstitial water (Roychoudhury, 2001). Here, however, all samples were rather fine and  
492 partially drained, with particle size measurements revealing a relatively small range in  
493 median particle diameter and surface area. Across such a small size range, additional,

494 confounding effects may be more significant among the samples that contribute to water  
 495 retention, such as variations in grain density, size distribution, organic matter content, degree  
 496 of consolidation and time-age of deposition.

497

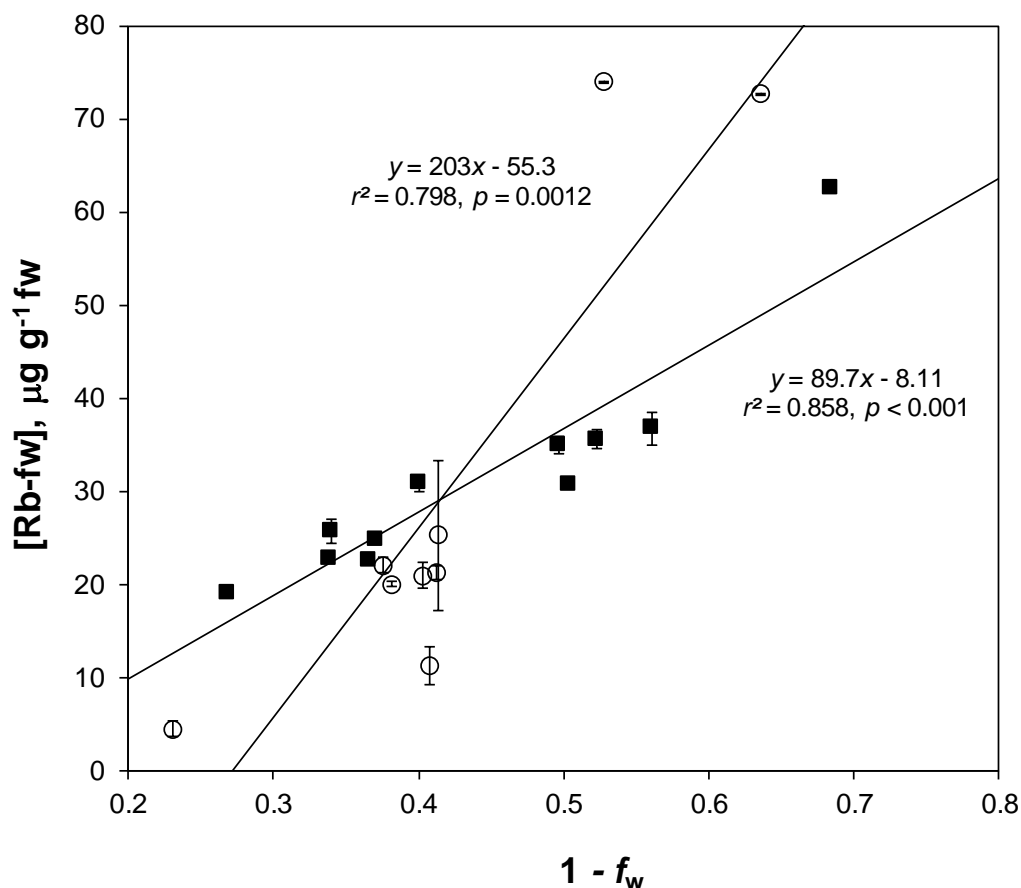
498 Regardless of the precise causes of the relationships observed, measurement of Rb appears to  
 499 provide a suitable, direct means of estimating interstitial water content provided that an  
 500 empirical calibration between [Rb-fw] and  $1 - f_w$  (with a slope,  $b$ , and intercept,  $a$ ) is  
 501 established for the environment of interest. In practice, therefore, the water-corrected metal  
 502 concentration on a dry weight basis, [Me-dw\*], may be calculated from the metal  
 503 concentration determined on a fresh weight basis and in the field, [Me-fw], as follows:

504 
$$[\text{Me-dw}^*] = \frac{[\text{Me-fw}]}{([\text{Rb-fw}] - a)/b} \quad (2)$$

505

$$([\text{Rb-fw}] - a)/b$$

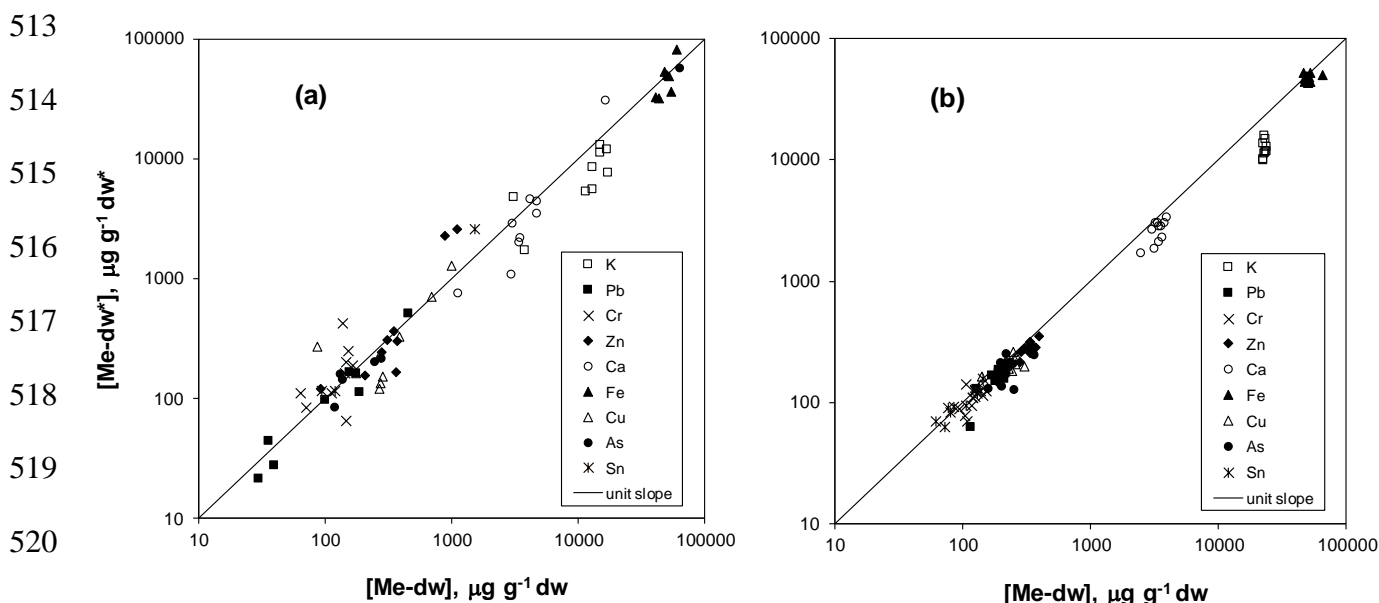
506



507



508 **Figure 5: Concentration of Rb determined on site and on a fresh weight basis ([Rb-fw],**  
 509  **$\mu\text{g g}^{-1}$  fw) versus  $1 - f_w$  for sediments from the axial transect of the Tamar (o) and the**  
 510 **inter-tidal transect of the Tavy (■). Errors represent the standard deviation about the**  
 511 **mean of six measurements and annotated are best-fit regression lines and results of**  
 512 **linear regression analysis.**

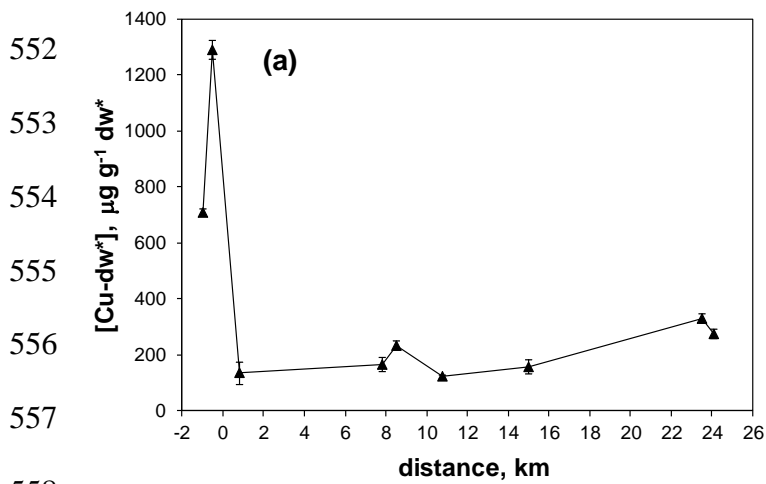


522 **Figure 6: Mean concentrations of metals measured on site and subsequently corrected**  
 523 **empirically according to equation 2 ( $[\text{Me-dw}^*]$ ,  $\mu\text{g g}^{-1}$   $\text{dw}^*$ ) versus corresponding mean**  
 524 **concentrations measured after freeze-drying ( $[\text{Me-dw}]$ ,  $\mu\text{g g}^{-1}$   $\text{dw}$ ) in the (a) Tamar**  
 525 **estuary and (b) Tavy estuary. Errors are not shown for clarity and the solid line**  
 526 **represents unit slope. Results of linear regression analysis were as follows: (a)  $y =$**   
 527  **$1.085x$ ,  $r^2 = 0.925$ ,  $p < 0.001$ ; (b)  $y = 0.862x$ ,  $r^2 = 0.954$ ,  $p < 0.001$ ; and after exclusion of**  
 528 **Ca and K data were: (a)  $y = 1.102x$ ,  $r^2 = 0.940$ ,  $p < 0.001$ ; (b)  $y = 0.923x$ ,  $r^2 = 0.987$ ,  $p <$**   
 529 **0.001.**

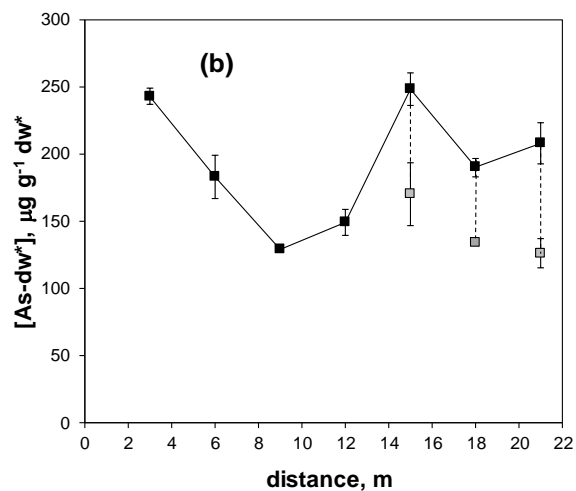
530  
 531 Direct, fresh weight measurements taken along the axis of the Tamar estuary and the transect  
 532 of the Tavy estuary were empirically corrected according to equation 2 and using the  
 533 coefficients defined in Figure 5 ( $a = -55.3$  and  $b = 203$ , and  $a = -8.11$  and  $b = 89.7$ ,

534 respectively) and are plotted against measurements made after freeze-drying in Figure 6.  
 535 Slopes of the best-fit lines defining all data points were within 15% of unit value and  
 536 regression coefficients exceeded 0.9 for both surveys and, as above, better fits and slopes  
 537 that were closer to unit value resulted when data for Ca and K had been excluded.  
 538  
 539 Results derived from this empirical approach are exemplified for specific elements in Figure  
 540 7. Thus, here, concentrations of Cu in surficial sediments are plotted as a function of distance  
 541 along the axis of the Tamar estuary and concentrations of As in surficial and anoxic (~ 5 cm  
 542 depth) sediments are shown as a function of distance across the mudflats of the Tavy estuary.  
 543 In the Tamar, distributions of Cu are consistent with two the principal sources of the metal:  
 544 inputs from a dense array of historical mine workings above the tidal limit (Mighanetara et  
 545 al., 2008), and a more diffuse input from boating activities (e.g. antifouling paint) towards  
 546 the mouth of the estuary (Turner, 2010). In the Tavy, distributions of As at the surface are  
 547 rather uniform, reflecting the homogenous dispersion of fine-grained material throughout the  
 548 intertidal zone; however, concentrations are significantly lower at depth (according to a  
 549 series of paired *t*-tests;  $\alpha = 0.05$ ) because of the dissolution of hydrous Fe oxide host phases  
 550 under reducing conditions (Chaillou et al., 2003).

551



558



559 **Figure 7: Mean metal concentrations measured on site and subsequently corrected**  
560 **empirically according to equation 2 ( $[Me-dw^*]$ ,  $\mu\text{g g}^{-1} dw^*$ ). (a) Cu in surficial**  
561 **sediments of the Tamar estuary as a function of axial distance from the tidal weir and**  
562 **(b) As in surficial sediments (filled squares) and anoxic sediments (shaded squares) as a**  
563 **function of distance from the high water mark. Errors represent the standard deviation**  
564 **about the mean of six measurements.**

565

566

### 567 *3.7. Concluding remarks*

568 The present study has shown that on site XRF analysis (using a Niton XL3t instrument)  
569 returns concentrations of metals in fine (milled), dried, particulate geosolids in a standardless  
570 mining mode with good accuracy over a range of concentrations typical of estuarine  
571 sediments. When samples are analysed fresh, however, the presence of water reduces signal  
572 intensity through both the dilution of material and the attenuation of exciting and fluorescent  
573 x-rays. While these effects can be corrected for empirically up to moisture contents of about  
574 60%, they impose constraints on the ability to determine dry-weight concentrations of metals  
575 directly in the field, with approximate values restricted to elements heavier than Cr and  
576 gained by assuming a generic fractional water content. A more practical means of  
577 determining the relative degree of metal contamination within or between estuaries,  
578 including axial distributions and localised transects, was to correct fresh-weight  
579 concentrations determined in the field with respect to Rb, an element that was  
580 simultaneously able to correct for both variations in granulometry and interstitial water  
581 content. This approach has the potential to detect subtle changes in trace metal  
582 contamination over small areas as well as more significant hot-spots of metals arising from  
583 localised sources. In the field, direct and immediate results may be used to guide a research

584 strategy, assist with rapid decision-making or target samples for further characterisation in  
585 the laboratory.

586

### 587 **Acknowledgements**

588 This study was partly funded by a HEIF Plymouth University Marine Institute grant. Drs  
589 Gillian Glegg and Charlotte Braungardt (PU) are thanked for assistance with sample  
590 collection.

591

### 592 **References**

593 Al-Jundi, J., 2001. Instrumental neutron activation analysis (INAA) of estuarine sediments.  
594 *Journal of Radioanalytical and Nuclear Chemistry* 249, 361-367.

595

596 Alyazichi, Y.M., Jones, B.G., McLean, E., Pease, J., Brown, H., 2017. Geochemical  
597 assessment of trace element pollution in surface sediments from the Georges River, Southern  
598 Sydney, Australia. *Archives in Environmental Contamination and Toxicology* 72, 247-259.

599

600 Azevedo, I., Ramos, S., Mucha, A.P., Bordalo, A.A., 2013. Applicability of ecological  
601 assessment tools for management decision-making: A case study from the Lima estuary  
602 (NW Portugal). *Ocean and Coastal Management* 72, 54-63.

603

604 Bull, A., Brown, M.T., Turner, A., 2017. Novel use of field-portable-XRF for the direct  
605 analysis of trace elements in marine macroalgae. *Environmental Pollution* 220, 228-233.

606

607 Cao, L.L., Huang, C.G., Wang, J.H., Xie, J., Ni, Z.X., Jin, G.X., Waxi, L.L., Chen, H.X.,  
608 2014. Pollution status of selected metals in surface sediments of the Pearl River estuary and  
609 Daya Bay, South China Sea. *Journal of Residuals Science and Technology* 11, 119-130.

610

611 Chaillou, G., Schäfer, J., Anschutz, P., Lavaux, G., Blanc, G., 2003. The behaviour of  
612 arsenic in muddy sediments of The Bay of Biscay (France). *Geochimica et Cosmochimica*  
613 *Acta* 67, 2993-3003.

614

615 Din, Z.B., 1992. Use of aluminium to normalize heavy-metal data from estuarine and coastal  
616 sediments of Straits of Melaka. *Marine Pollution Bulletin* 24, 484-491.

617

618 Ge, L., Lai, W., Zhou, S., Ren, J., Lin, L., Lin, Y., 2001. New XRF probe for in situ  
619 determination of concentration of multi-elements in ocean sediments. *Chengdu Ligong*  
620 *Xueyuan Xuebao* 28, 80–85.

621

622 Ge, L., Lai, W., Lin, Y., 2005. Influence of an correction for moisture in rocks, soils and  
623 sediments on in situ XRF analysis. *X-ray Spectrometry* 34, 28-34.

624

625 Higuera, P., Oyarzun, R., Iraizoz, J.M., Lorenzo, S., Esbrí, J.M., Martínez-Coronado, A.,  
626 2012. Low-cost geochemical surveys for environmental studies in developing countries:  
627 Testing a field portable XRF instrument under quasi-realistic conditions. *Journal of*  
628 *Geochemical Exploration* 113, 3-12.

629

630 Hubbell, J.H., Seltzer, S.M., 1996. X-ray mass attenuation coefficients. National Institute of  
631 Standards and Technology, Gaithersburg, Maryland.

632

633 Kennish, M.J., 1998. Trace metal-sediment dynamics in estuaries: Pollution assessment.  
634 *Reviews in Environmental Contamination and Toxicology* 155, 69-110.

635

636 Kirtray, V.J., Kellum, J.H., Apitz, S.E., 1998. Field-portable X-ray Fluorescence  
637 Spectrometry for metals in marine sediments: Results from multiple sites. *Water Science and*  
638 *Technology* 37, 141-148.  
639  
640 Lemiere, B., Laperche, V., Haouche, L., Auger, P., 2014. Portable XRF and wet materials:  
641 application to dredged contaminated sediments from waterways. *Geochemistry –*  
642 *Exploration Environment Analysis* 14, 257-264.  
643  
644 Loring, D.H., 1991. Normalization of heavy-metal data from estuarine and coastal  
645 sediments. *ICES Journal of Marine Science* 48, 101–115.  
646  
647 Mejía-Piña, K.G., Huerta-Diaz, M.A., González-Yajimovich, O., 2017. Calibration of  
648 handheld X-ray fluorescence(XRF) equipment for optimum determination of elemental  
649 concentrations in sediment samples. *Talanta* 161, 359-367.  
650  
651 Mighanetara, K., Braungardt, C.B., Rieuwerts, J.S., Azizi, F., 2009. Contaminant fluxes  
652 from point and diffuse sources from abandoned mines in the River Tamar catchment, UK.  
653 *Journal of Geochemical Exploration* 100, 116-124.  
654  
655 Mucha, A.P., Vasconcelos, M.T.S.D., Boralo, A.A., 2004. Vertical distribution of the  
656 macrobenthic community and its relationships to trace metals and natural sediment  
657 characteristics in the lower Douro estuary, Portugal. *Estuarine and Coastal Shelf Science* 59,  
658 663-673.  
659

660 Nolting, R.F., Ramkema, A., Everaats, J.M., 1999. The geochemistry of Cu, Cd, Zn, Ni and  
661 Pb in sediment cores from the continental slope of Banc d'Arquin (Mauritani). *Continental*  
662 *Shelf Research* 19, 665-691.

663

664 Parsons, C., Grabulosa, E.M., Pili, E., Floor, G.H., Roman-Ross, G., Charlet, L., 2013.  
665 Quantification of trace arsenic in soils by field-portable x-ray fluorescence spectrometry:  
666 Considerations for sample preparation and measurement conditions. *Journal of Hazardous*  
667 *Materials* 262, 1213-1222.

668

669 Quiroz-Jiménez, J.D., Roy, P.D., 2017. Evaluation of geochemical data by two different  
670 XRF spectrometers in sediments from the Santiaguillo Basin (state of Durango, Mexico).  
671 *Geofísica Internacional* 56, 305-315.

672

673 Radu, T., Diamond, D., 2009. Comparison of soil pollution concentrations determined using  
674 AAS and portable XRF techniques. *Journal of Hazardous Materials* 171, 1168–1171.

675

676 Rae, J.E., 1997. Trace metals in deposited intertidal sediments. In: *Biogeochemistry of*  
677 *Intertidal Sediments*, ed. T.D. Jickells and J.E. Rae, Cambridge University Press, pp.16-41.

678

679 Regnier, P., Arndt, S., Goosens, N., Volta, C., Laruelle, G.G., Lauerwald, R., Hartmann, J.,  
680 2014. Modelling estuarine biogeochemical dynamics: From the local to the global scale.  
681 *Aquatic Geochemistry* 19, 591-626.

682

683 Roychoudhury, A.N., 2001. Dispersion in unconsolidated aquatic sediments. *Estuarine,*  
684 *Coastal and Shelf Science* 53, 745-757.

685

686 Stallard, M.O., Apitz, S.E., Dooley, C.A., 1995. X-ray fluorescence spectrometry for field  
687 analysis of metals in marine sediments. *Marine Pollution Bulletin* 31, 297-305.

688

689 Tjallingii, R., Röhl, U., Kölling, M., Bickert, T., 2007. Influence of the water content on x-  
690 ray fluorescence core-scanning measurements in soft marine sediments. *Geochemistry,*  
691 *Geophysics, Geosystems* 8, Q02004, doi:10.1029/2006GC001393.

692

693 Turner, A., 2010. Marine pollution from antifouling paint particles. *Marine Pollution*  
694 *Bulletin* 60, 159-171.

695

696 Turner, A., 2017. In situ elemental characterisation of marine microplastics by portable  
697 XRF. *Marine Pollution Bulletin* 124, 286-291.

698

699 Turner, A., Lewis, M., 2018. Lead and other heavy metals in soils impacted by exterior  
700 legacy paint in residential areas of south west England. *Science of the Total Environment*  
701 619-620, 1206-1213.

702

703 Turner, A., Millward, G.E., 2002. Suspended particles: Their role in estuarine  
704 biogeochemical cycles. *Estuarine Coastal and Shelf Science* 55, 857-883.

705

706 Turner, A., Poon, H., Taylor, A., Brown, M.T., 2017. In situ determination of trace elements  
707 in *Fucus* spp. by field-portable-XRF. *Science of the Total Environment* 2017, 593-594, 227-  
708 235.

709

710 Wei, R., Haraguchi, H., 1999. Multielement determination of major-to-ultratraces elements in  
711 river and marine sediment reference materials by inductively coupled plasma atomic  
712 emission spectrometry and inductively coupled plasma mass spectrometry. *Analytical*  
713 *Sciences* 15, 729-735.

714

715 Zhao, G., Ye, S., Yuan, H., Ding, X., Wang, J., 2017. Surface sediment properties and heavy  
716 metal pollution assessment in the Pearl River Estuary, China. *Environmental Science and*  
717 *Pollution Research International* 24, 2966-2979.



